ADVANCED MATERIALS TECHNOLOGIES
www.advmattechnol.de

Correlative Analysis of Intra- Versus Extracellular Cell Detachment Events via the Alignment of Optical Imaging and Detachment Force Quantification

*Franziska Weigl, Carina Blum, Ana Sancho, and Jürgen Groll**

In recent decades, hybrid characterization systems have become pillars in the study of cellular biomechanics. Especially, Atomic Force Microscopy (AFM) is combined with a variety of optical microscopy techniques to discover new aspects of cell adhesion. AFM, however, is limited to the early-stage of cell adhesion, so that the forces of mature cell contacts cannot be addressed. Even though the invention of Fluidic Force Microscopy (FluidFM) overcomes these limitations by combining the precise force-control of AFM with microfluidics, the correlative investigation of detachment forces arising from spread mammalian cells has been barely achieved. Here, a novel multifunctional device integrating Fluorescence Microscopy (FL) into FluidFM technology (FL-FluidFM) is introduced, enabling real-time optical tracking of entire cell detachment processes in parallel to the undisturbed acquisition of force-distance curves. This setup, thus, allows for entailing two pieces of information at once. As proof-of-principle experiment, this method is applied to fluorescently labeled rat embryonic fibroblast (REF52) cells, demonstrating a precise matching between identified force-jumps and visualized cellular unbinding steps. This study, thus, presents a novel characterization tool for the correlated evaluation of mature cell adhesion, which has great relevance, for instance, in the development of biomaterials or the fight against diseases such as cancer.

1. Introduction

In the last two decades, Atomic Force Microscopy (AFM) has emerged as one of the most powerful characterization tools in material science. After revolutionizing the surface-imaging by visualizing structures in a nanometer range, AFM became increasingly important in addressing diverse biological questions, like protein-DNA interactions[1] or characteristics of cell adhesion.[2] Especially, the latter one was of great interest, since the attachment of cells to an extracellular matrix (ECM) or another cell plays a crucial role in fundamental biological processes, like tissue growth,[3] cell-biomaterial interactions,[4] or the origin and progression of diseases such as cancer.[5] To investigate cell adhesion forces under near-physiological conditions, AFM was combined with the highly sensitive Single-Cell Force Spectroscopy (SCFS) allowing the quantification of unbinding forces of receptor/ligand bonds or of whole cell adhesion.[6] More precisely, a cell is chemically attached to a functionalized cantilever and approached towards a surface or another cell, followed by immobilization and retraction after several seconds to minutes.[6b] During this procedure, cantilever deflection is recorded over time resulting in a so-called force-distance curve. Therefore, this experimental protocol enables the quantification of adhesion forces in a range of ≈10 pN to ≈100 nN making AFM-based SCFS the standard method for studying cellular adhesion over several years.[6b,7]

Besides the advances in the quantitative investigation of biomechanics using AFM-based SCFS, the field of Fluorescence Microscopy (FL) also became one of the key pillars in the characterization of cell adhesion.[8] Moreover, the innovative development of diverse Super-Resolution (SR) microscopy techniques like Stimulated Emission Depletion (STED) microscopy or direct Stochastic Optical Reconstruction Microscopy (*d*STORM) revolutionized the optical monitoring by visualizing single proteins within a resolution of a few nanometers.[9] However, none of these well-established techniques alone can address and encompass the complexity of cell adhesion. Therefore, the complementary combination of AFM with diverse optical methods such as Total Internal Reflection FL (TIRFM),[10] Super-Resolution Structured Illumination Microscopy (SR-SIM),[11] or

F. Weigl, C. Blum, A. Sancho,[+] J. Groll
Department for Functional Materials in Medicine and Dentistry at the Institute of Functional Materials and Biofabrication and Bavarian Polymer Institute
University of Würzburg
Pleicherwall 2, D-97070 Würzburg, Germany
E-mail: juergen.groll@fmz.uni-wuerzburg.de

The ORCID identification number(s) for the author(s) of this article can be found under https://doi.org/10.1002/admt.202200195.

[+]Present address: Department of Automatic Control and Systems Engineering, University of the Basque Country UPV/EHU, Plaza de Europa 1, Donostia 20018, Spain

DOI: 10.1002/admt.202200195

*d*STORM[12] has taken over an increasingly important role in the understanding of cellular biomechanics in the last decades. Nevertheless, the data acquisition of these correlative methods is mostly performed subsequentially and superimposed afterwards due to interference of AFM cantilever and fluorescence excitation light.[8,11,13] However, recently, Fernandes et al. (2020) realized a correlative and truly simultaneously operational scheme of AFM Force Spectroscopy (AFM-FS) and confocal Fluorescence Lifetime Imaging Microscopy (FLIM) and therefore, took the development of novel multifunctional devices to the next level.[8]

Nevertheless, there are shortcomings in the experimental performance of AFM that cannot be addressed or overcome by implementing optical microscopy. One of the main limitations is the restriction on early-stage adhesion.[5c,6,14] To overcome this constraint, Fluidic Force Microscopy (FluidFM) was established by Zambelli's group in 2009.[15] It combines the precise force-controlled positioning with the versatility of microfluidics, incorporating an external pumping system which is connected to the cantilever via a microchannel.[15,16] Thus, a pressure-modulated cell immobilization enables the study of mature cell contacts, whose adhesion forces would normally exceed the chemical binding-force between a cell and a functionalized AFM cantilever.[6b,17] Since then, FluidFM-based SCFS became the gold-standard method for investigating cell adhesion of spread eukaryotic and prokaryotic cells, realizing a force quantification in the range of piconewton (pN) to several micronewtons (μN).[5c,17,18] In this overall framework, the research field of mechanobiology experienced great advancements through the establishment of diverse multifunctional AFM systems as well as the further development of the FluidFM technology. However, the question of optical tracking of the corresponding biomechanical and complex processes remains unanswered.

Here, we introduce a multifunctional device correlating FL and FluidFM technology (FL-FluidFM), which enables the visualization of cellular detachment and, at the same time, the quantification of corresponding detachment forces. By implementing a piezo-driven objective positioner (PIFOC) and an immersion oil objective, we achieved high focus stability with optimized optical resolution throughout the entire experiment. Furthermore, the use of fluorescent excitation light with a wavelength of 555 nm revealed no meaningful interference in either optical tracking or force quantification. Using fluorescently labeled rat embryonic fibroblast (REF52) cells for proof-of principle examination, we pioneer and explore complete cell detachment processes while truly simultaneously recording the corresponding detachment forces. Moreover, we established a protocol for unambiguous matching between quantified force-jumps and the visualized steps of cellular unbinding. Consequently, we believe that this technological correlation paves the way toward a novel characterization method and, therefore, provides new insights into the complex biomechanics of cell adhesion.

2. Results

2.1. Design and Fabrication of the Correlated FL-FluidFM Device

In this study, we established a customized and correlated system, which combines FL and FluidFM technology (FL-FluidFM), enabling real-time monitoring of cellular detachment with simultaneously recording the corresponding detachment forces. **Figure 1**a shows a schematic setup of this in-house developed device, initially based on a standard FluidFM setup as described in Sancho et al. (2017).[5c] Thus, the novel system is based on a scan head (FlexAFM V5+ SLD, Nanosurf GmbH, Langen, Germany) combining AFM with FluidFM technology (Cytosurge AG, Glattbrugg, Switzerland), mounted on an inverted fluorescence microscope (Axio-Observer Z1, Carl ZEISS AG, Oberkochen, Germany) which carries a piezoelectric sample stage of 100 μm retraction range (npoint LC400 controller, Nanosurf GmbH, Langen, Germany). Concerning the desired high-precision monitoring of cell detachments, the optimization of the optical components was crucial. Therefore, a high numerical immersion oil objective (Plan-Apochromat 40x/1.4 Oil DICIII, Carl ZEISS AG, Oberkochen, Germany), as well as a piezo-driven PIFOC (Piezo Flexure Objective Positioner) system (nanoFaktur GmbH, Villingen-Schwenningen, Germany), was implemented, providing high optical resolution and focus stability throughout an experiment (Figure 1b). The latter aspect is achieved by a synchronous movement of sample stage and objective, constantly regulated via a closed feedback-loop and, thus, ensuring a precisely guided motion with a resolution in the nanometer range (Figure 1c). For a simultaneous visual control over the cantilever alignment and the FL, the output signal is directed to two independent cameras via a reversible 50:50 beam splitter. The acquisition of fluorescence signal is accomplished using a monochromatic CCD camera (AxioCam MRm, Carl ZEISS, Oberkochen, Germany) while laser spot alignment of the FluidFM is performed with a CMOS camera (UI-3060CP-M-GL Rev.2, IDS Imaging Development Systems GmbH, Obersulm, Germany). A light emitting diode (LED) light source (Colibri 7, Carl ZEISS AG, Oberkochen, Germany) was implemented for the fluorescent illumination, providing up to seven fluorescence excitation lines and fast channel switching in the range of microseconds. By integrating a high-efficiency filter set (90 HE LED Carl ZEISS AG, Oberkochen, Germany), four excitation wavelengths (385/475/555/630 nm) are available simultaneously. To shield any noise, the whole FL-FluidFM system is placed on a vibration isolation base (Accurion Halcyonics-i4, Accurion GmbH, Göttingen, Germany) and covered by an acoustic protection box.

2.2. Visualization of Cell Detachments with Optimized Focus Stability and High Optical Resolution

One of the most important steps towards a real-time visualization of cell detachment processes was achieving high optical resolution and high focus stability. For this, the implementation of a high numerical immersion oil objective combined with a PIFOC system was crucial (Figure 1c). **Figure 2** shows a comparison of visualized cell detachments of single REF52 cells without (Figure 2a–c) and with (Figure 2d–f) optimized microscopic optical hardware components. It is obvious that the performance of the standard FluidFM device provides a low optical resolution and no focus stability, which can be referred to as the lack of focus control. Thus, optical tracking of the cellular movements during a detachment is nearly impossible.

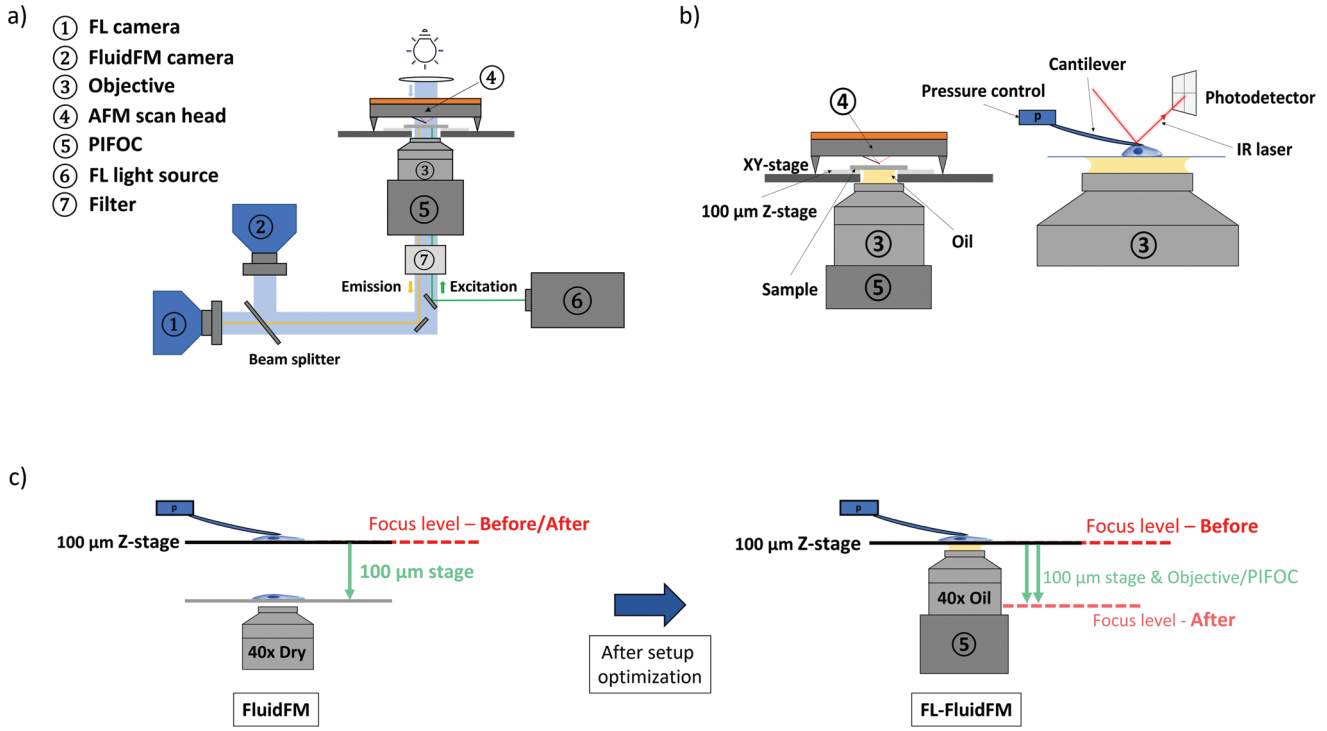

Figure 1. Schematic setup of a customized FL-FluidFM system. a) Correlated FL-FluidFM device based on an AFM scan head that is connected to a monochromatic LED light source for fluorescence illumination. b) Detailed view of the interface between sample and high numerical objective mounted on a PIFOC system. c) Comparison of focus stability without (FluidFM) and with (FL-FluidFM) PIFOC implementation.

In contrast, using a PIFOC system results in high focus stability during the entire measurement (Figure 2d–f). Here, the interface between cell and substrate stays in the focal plane until the cell is fully detached (Figure 2f), enabling a detailed visualization of an entire unbinding process. In addition to the achievement of high focus stability, the implementation of an immersion oil objective entailed high optical resolution, which is especially beneficial for the more detailed analysis of intracellular movements during cellular de-adhesion. Finally, the optimization of microscopic visualization components seems

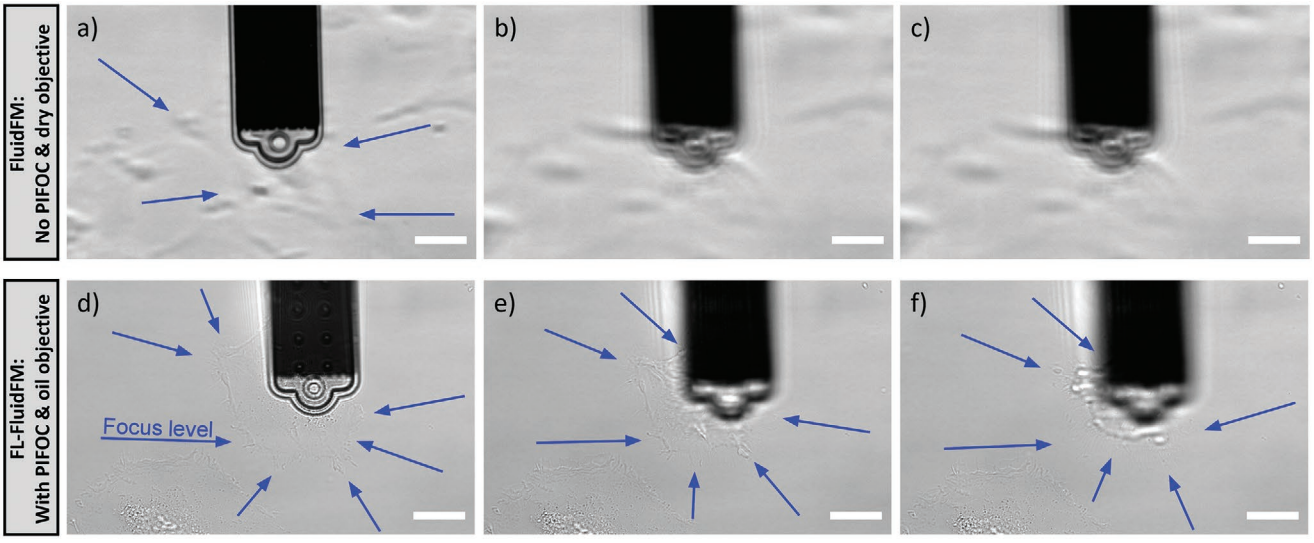

Figure 2. Comparison of the focus stability and optical resolution between standard a–c) FluidFM and d–f) FL-FluidFM setup: both cases show a composition of three brightfield images taken at the beginning, in the middle, and at the end of a cell detachment experiment. Blue arrows mark the respective cell which will be detached. (a–c) Images taken with the commonly used FluidFM system show reduced optical resolution and a loss in focus. (d–f) Brightfield images illustrate the high optical resolution and high focus stability of a detachment process which was monitored using the correlated FL-FluidFM device. Scale bar: 20 µm.

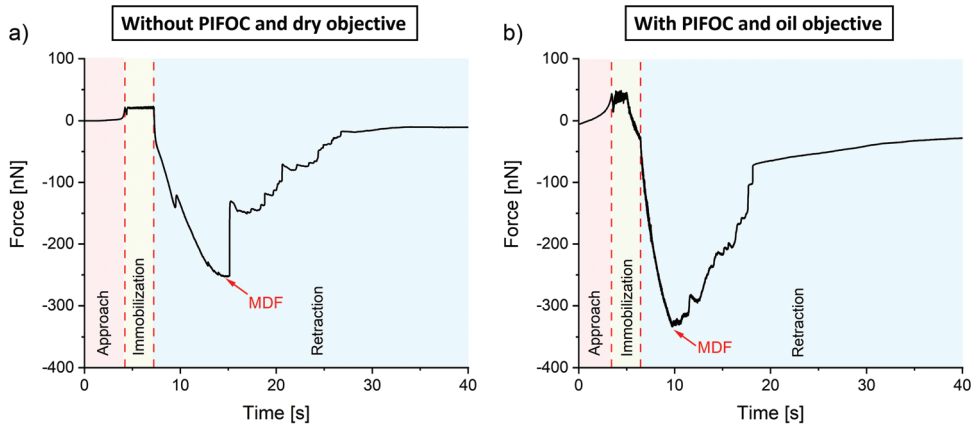

Figure 3. Exemplary force-curves of REF52 cell-detachment experiments a) before and b) after optimization of focus stability and optical resolution. Both measurements show an MDF at the highest point of force and several force-steps. Both experiments were recorded under brightfield illumination: (a) The exemplary force-curve of a detached REF52 cell, which was recorded with the standard FluidFM device. (b) The force-curve of a cell that was detached from a substrate using the correlated FL-FluidFM system.

to pave the way for the first time to a real-time and correlated investigation of cellular insights and cell adhesion forces during a cell detachment experiment.

2.3. Verification of FluidFM Functionality after Successful Adaptation of Focus Control and Optical Resolution

After successfully advancing the device by implementing the PIFOC and the oil immersion objective, the functionality of the setup was validated. Here, the focus was on the occurrence of noise caused by the additional component of mechanical motion when simultaneously positioning a PIFOC-controlled objective and the sample stage. This in turn can affect the highly sensitive force measurements. Furthermore, the oil film between objective and substrate could offer a direct transmission path of vibrations into the experimental medium surrounding the cantilever and thus also onto the cantilever itself. To ensure that vibrations do not negatively influence the high-sensitive measurement procedure of the FluidFM technology, SCFS was performed by using the novel and focus-controlled as well as the standard FluidFM device. In short, every single cell detachment force-curve is composed of three sections: approach, immobilization, and retraction (**Figure 3**), as already described by Sancho et al. (2017).[5c] In the first phase, cantilever and targeted cell are brought into contact (approach, red section), followed by the application of a constant suctioning pressure to immobilize the cell at the cantilever tip (immobilization, green section). The last phase shows a retraction curve, which demonstrates the typical process of a cellular detachment (retraction, blue section). Here, the force increases within a few seconds until the so-called Maximum Detachment Force (MDF) is reached. This is followed by multiple detachment steps, occurring as abrupt force-jumps. After complete cell detachment, the force returns to a minimum with a slight shift towards negative values. This is due to viscous drag and the additional weight of the attached cell, hindering the cantilever deflection to return to its initial state.

Figure 3 illustrates the exemplary force-curve of a detached REF52 cell using either the standard FluidFM (Figure 3a) or the correlated FL-FluidFM (Figure 3b) setup without and with PIFOC and oil immersion objective, respectively. Both curves show a comparable force progression of approach, immobilization, and retraction with respect to the precision of the method. Especially the third section, which is the most important one for cell adhesion analysis, reveals a high number of multiple unbinding events in both cases. Also, the two MDFs are in the same order of magnitude when considering their standard deviations (FluidFM: (−253 ± 75) nN and FL-FluidFM: (−334 ± 91) nN)). The overall course of detachment forces was measured for more than ten cells with both systems (Figure S1a,b, Supporting Information), indicating no apparent negative influence on data acquisition using the advanced FL-FluidFM that can be attributed to the implementation of PIFOC or high numerical objective. Therefore, the highly sensitive data acquisition of force-curves using the correlated FL-FluidFM system was verified.

2.4. Integration of Fluorescence Illumination for the Visualization of Cellular Components During Cell Detachment

After the successful implementation of PIFOC and high numerical objective, the next step in establishing a correlated FL-FluidFM setup was the concurrent fluorescent visualization of cellular insights. For this purpose, fluorescence illumination was integrated into the experimental procedure. Together with the high focus stability, we thus achieved a real-time optical tracking of fluorescently labeled cellular components using live-cell staining. Therefore, REF52 cells stably expressing paxillin-yellow fluorescent protein (YFP) as one of the well-known focal adhesion proteins,[19] were additionally transiently transfected with LifeAct-mCherry to fluorescently label the F-actin cytoskeleton. **Figure 4**a shows an example of a dual-fluorescently labeled cell under brightfield illumination, well-aligned towards the cantilever. The fluorescently labeled paxillin (Figure 4b) and F-actin filaments (Figure 4c) are illustrated in green and orange signals, respectively. In addition, the overlay image (Figure 4d) demonstrates a spread cell morphology with paxillin allocated

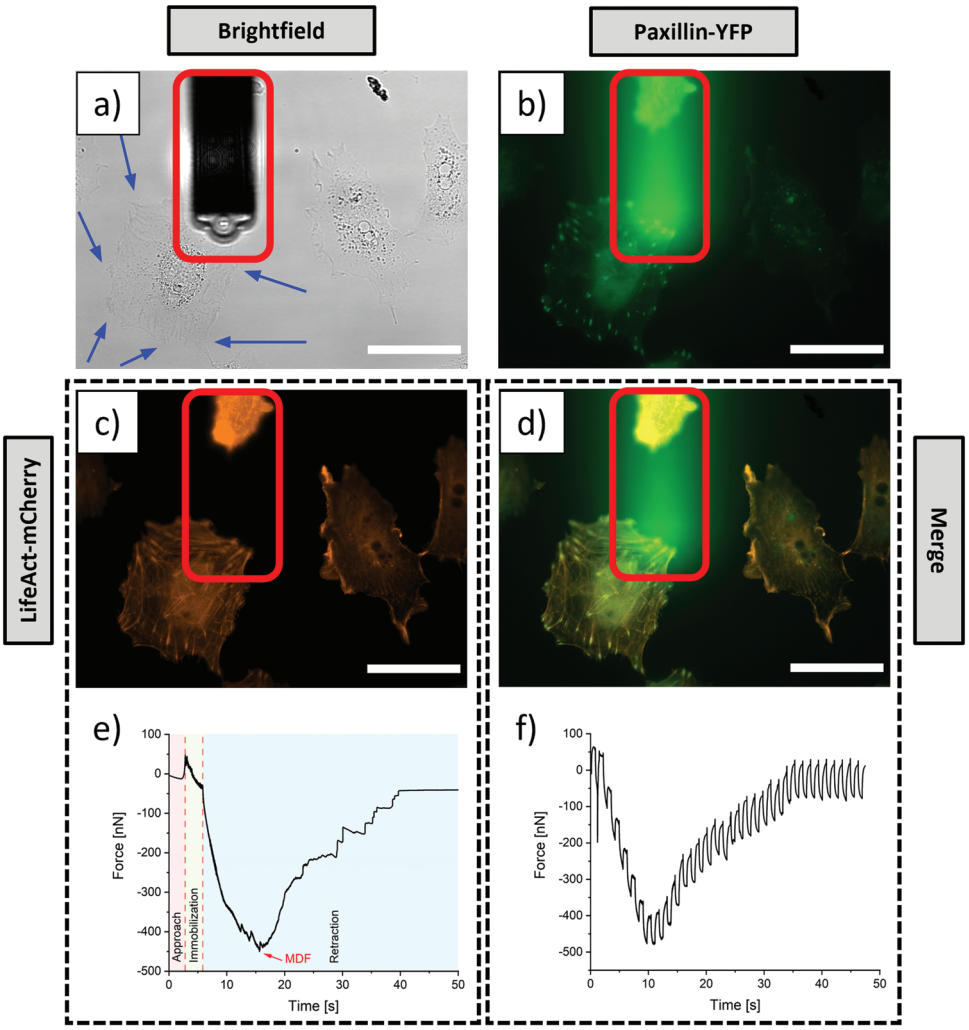

Figure 4. Integration of fluorescence illumination into the correlated data acquisition using FL-FluidFM: a) A REF52 cell stably expressing paxillin-YFP and transiently transfected with LifeAct-mCherry (F-actin) is visualized with brightfield illumination. The position of the cantilever is marked with a red square. The blue arrows point to the edge of the targeted cell. b) The fluorescence image reveals green, fluorescent paxillin signal but also a strong cantilever luminescence. c) The fluorescence image of the cell shows no detectable cantilever autoluminescence but clearly visible F-actin filaments, illustrated with orange signal. d) The dual-fluorescence image of the REF52 cell demonstrates the overlay signal of paxillin-YFP and LifeAct-mCherry. The green autoluminescence of the cantilever is clearly visible in this case. e) The force-curve that was recorded simultaneously to the F-actin visualization is separated into the typical sections of approach, immobilization, and retraction and shows no obvious disturbance due to spurious cantilever bending. f) The force-curve acquired under dual-fluorescence illumination exposes a strong sinusoidal signal overlaying the whole detachment process. Scale bar: 50 µm.

at the ends of elongated actin filaments. After the successful establishment of this live-cell labeling, we realized the optical tracking of an entire cell detachment process under fluorescence illumination, which, to the best of our knowledge, has not been reported yet.

However, although fluorescence images were recorded using dual-fluorescence illumination, the correlated acquisition of FL-FluidFM data was performed only with one excitation light at a time. This is because simultaneous application of fluorescence light and SCFS caused non-linear cantilever deflection and/or autoluminescence (Figure 4). In our system, especially the excitation light of paxillin (475 nm) triggered a pronounced cantilever autoluminescence (Figure 4b,d). By contrast, illumination with 555 nm did not induce any luminescence effect, enabling a detailed visualization of intracellular F-actin (Figure 4c). Moreover, the simultaneous visualization of actin filaments and force quantification revealed no interference signal indicating a spurious cantilever bending (Figure 4e). Analogous to the curve recorded with brightfield illumination (Figure 3b), Figure 4e exhibits the typical force progression of a cellular detachment with an MDF in the same order of magnitude as described in Section 2.3 ((–450 ± 136) nN). In contrast, dual-excitation light irradiation of a cell detachment experiment resulted in a sinusoidal signal overlapping the entire force-curve and, therefore, making the analysis of cellular unbinding events impossible (Figure 4f). Consequently, all correlated FL-FluidFM experiments were performed using only the orange fluorescence

signal, ensuring a high-quality visualization and quantification of cell detachment processes at the same time. Finally, the fluorescence illumination was successfully integrated into the cellular detachment process without negatively affecting the data quality of force-curves.

2.5. Correlated Analysis of FL-FluidFM Data

The above experiments have successfully demonstrated the feasibility of a correlated investigation of cell adhesion using FL-FluidFM technology. Here, the correlated hardware performance of FL and FluidFM technology enables the simultaneous recording of force-curves and visualization of cellular detachment. Consequently, the next step was to analyze this correlated data, focusing on the achievement of a specific matching between force-steps and visible unbinding events within a cell. **Figure 5**a shows an exemplary force-curve of a detached REF52 cell. Here, each visible force-jump was marked by a linear fit, shown by purple lines. The last step before a complete detachment was chosen as a time-dependent reference point between force-curve and corresponding time-series to correlate the force-jumps with visible unbinding events. A specific step-matching was feasible by comparing the time points given by the force-jumps with the moment of visible cellular unbinding. The number of force-steps, which could be referred to as certain unbinding events within an optically tracked cell, is shown in Figure 5b, with all 20 steps highlighted with purple lines. The corresponding fluorescence image of the cell showing each identified spot of intracellular unbinding (arrow 1–20) is illustrated in Figure 5c. To further demonstrate the observed detachment process, Figure 5d shows a step-by-step image composition, highlighting the individual unbinding spots of actin filaments with arrows. This time-resolved process (Video S1, Supporting Information) shows the movement of the cytoskeleton during the detachment process that initially starts in the middle of the cell body (steps 1–10), where it is immobilized at the cantilever tip. Then, the cytoskeletal unbinding spreads from the inside to the outside, until there is only contact between cellular edge and surface (steps 11–20). After completely separating the cell from its substrate, there is no further detectable fluorescence signal in the focus level. This whole procedure correlates with the morphological movements observed under brightfield illumination (Video S2, Supporting Information).

Furthermore, comparing this described procedure of cellular de-adhesion with the fitted force-steps in (Figure 5a),

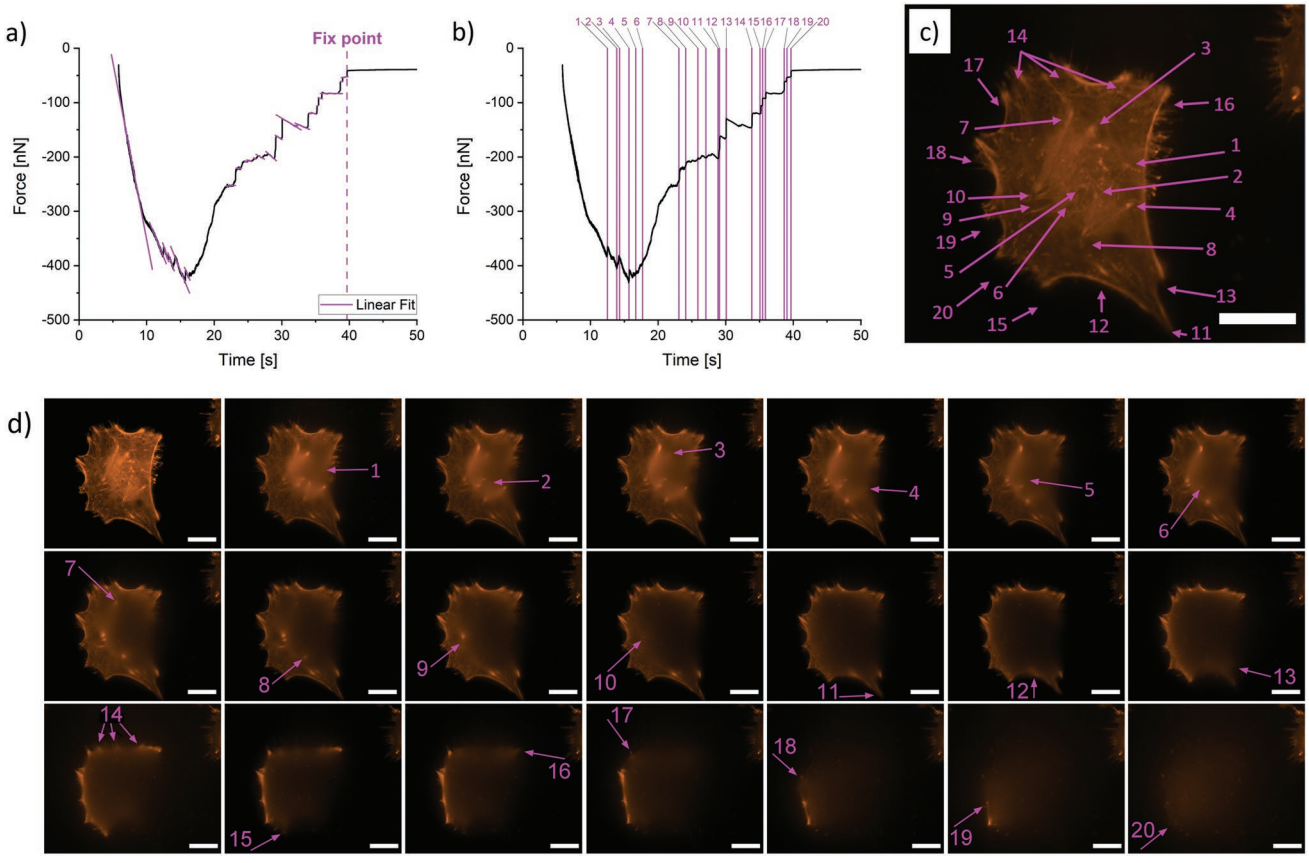

Figure 5. Correlated data analysis of an exemplary detachment experiment in which the unbinding process of a REF52 cell was performed using the correlated FL-FluidFM technology: a) The exemplary force-curve shows linear fits of single force-jumps, which were marked with purple lines. The last force step serves as a fixed reference point (purple dashed line). b) The purple lines sign each force-jump that could be attributed to a certain unbinding event visible in the corresponding fluorescence time-series (c and d) of the detachment process. c) The corresponding spots of cellular unbinding are marked with purple arrows and the matching number. d) A step-by-step image composition of the time-series recorded during the detachment process showing the position of the 20 identified unbinding events in (c). Scale bar: 20 µm.

a correlation between the area of filamentous unbinding and slope distribution could be assumed. At the beginning of a detachment process, when the intracellular unbinding dominates, the degree of slope is relatively high (Figure S2, Supporting Information). After exceeding the MDF, the linear slope slowly decreases and settles at a value around zero, when the cell is fully separated from its substrate. During this transition, the visible cellular unbinding also shifts from the inside to the cellular edge, indicating a correlation between the force-jumps' gradient and the filamentary unbinding area. Evaluating this correlated data analysis, it can be concluded that the FL-FluidFM technology enables a clear link between force-steps and cellular unbinding events and, therefore, opens a novel pathway for investigating cell adhesion.

3. Discussion

This study aimed to correlate FluidFM technology and FL within one setup. Already 2012, *Nature* has highlighted the advantages of correlative microscopy by declaring two microscopes are better than one.[20] Especially AFM was combined with a variety of optical microscopy techniques like TIRFM[10b,21] or *d*STORM[12] providing remarkable advances in biological research. However, the non-feasibility of simultaneous data acquisition, as well as the restriction of AFM to early-stage adhesion, represented a major drawback.[13] Thus, the FluidFM technology was developed by Zambelli's group in 2009.[15] Besides its application for intracellular injection[22] and pick-and-place experiments,[18a,23] FluidFM has become the gold-standard method for investigating mature cell adhesion.[5c,16,24] Nevertheless, to the best of our knowledge, a multifunctional system that enables the quantification and visualization of mature cell adhesion at the same time is still lacking. To fill this gap, a novel in-house developed device correlating FluidFM technology and FL and, therefore, paving the way towards real-time optical tracking of cellular detachment, was presented in this study.

One of the basic requirements for establishing this correlated device was a high optical resolution and high focus stability throughout an entire cell detachment experiment. Analogous to the study of Puech et al. (2006),[2a] we implemented a PIFOC system into our device, which enabled a piezo-controlled positioning of the objective's focal plane, synchronized to the vertical movement of the 100 µm Z-stage. In addition, with the integration of a high numerical objective whose application is already well-established in the context of correlative SR-AFM microscopy,[11,12,25] we achieved a high-resolution visualization of cell detachment and corresponding unbinding processes (Figure 2d–f). However, although these components are already widely used in microscopic apparatus, it was the first time to be integrated into a FluidFM-based microscope. Therefore, cell-detachment experiments were performed assessing the recorded data of the standard and the optimized device, to verify the functionality of the highly sensitive FluidFM performance after hardware modification.

Comparing the shape of the two exemplary force-curves (Figure 3a,b) with the ones of other studies,[4b,5c,13b,24] no remarkable difference was visible. Both show the typical way of detachment including approach, immobilization, and retraction with the characteristic force-pattern of cellular unbinding. Only the slight difference in MDF, representing the highest point of cell-substrate binding,[4b] is noticeable, which at first glance could be explained with the individuality of each cell regarding size and, therefore, contact area, stiffness, or the number of focal contact points.[4b,26] However, by comparing the respective totality of cells recorded with or without improved optics (Figure S1a,b, Supporting Information), it is apparent that the cells investigated with the new hardware have with (–467 ± 105) nN an overall higher MDF on average than the ones investigated with the standard FluidFM (MDF_{mean} = (–219 ± 78) nN). To further analyze a possible effect of the setup adjustment, additional measurements were carried out only with an oil objective and without the PIFOC system (Figure S1c, Supporting Information). Here, the average MDF was with (–281 ± 98) nN in the same range as the one measured with the standard FluidFM device. However, considering the already mentioned and well-established use of PIFOC and immersion oil objective in correlative microscopy, an impact on the quality of FluidFM performance is very unlikely. Thus, this discrepancy can be most probably explained by the mathematical proportionality between force and different cantilever parameters (Equation 1). Although all measurements were based on the same cantilever type and on the same calibration method, the calibrated spring constant k_{Calib} of the used cantilevers revealed a remarkable difference, while the calibrated deflection sensitivities δ_{Calib} (without PIFOC: $\delta_{Calib} = 8.56 \times 10^{-8}$ m V^{-1}, with PIFOC: $\delta_{Calib} = 8.31 \times 10^{-8}$ m V^{-1}) were in the same order of magnitude. Therefore, the measurement of low MDFs was connected to a cantilever with a calibrated spring constant of 1.25 N m^{-1}, whereas high MDFs were quantified with a cantilever of 2.55 N m^{-1} calibrated spring constant, leading to an overall much higher force. Considering this mathematical relationship directly influencing the accuracy of SCFS data,[27] it is very likely that the high difference in cantilever stiffness is responsible for the discrepancy between the mean MDFs instead of the implementation of PIFOC or oil objective. Moreover, by comparing the original MDFs recorded with PIFOC with the ones calculated with the cantilever parameters used for the measurements without PIFOC, a clear decrease in force is visible (Figure S3, Supporting Information). Here, the average MDF of (–236 ± 53) nN is in the same range as the ones without PIFOC. Therefore, it can be stated that neither the modification of the device nor the biological diversity of the cells is the decisive factor for the overall increase in MDF after setup optimization. Moreover, it can be concluded that the integration of PIFOC and oil objective allowed a real-time optical tracking of cellular detachment with extraordinary focus stability and high optical resolution for the first time.

After successfully optimizing the optical hardware design, we further integrated the fluorescence illumination into the workflow of cell detachment. We successfully demonstrated the simultaneous fluorescent visualization and detachment force quantification of fluorescently labeled REF52 cells as proof-of-principle experiments. The exemplary force-curve illustrated in Figure 4e shows the same way of force-pattern compared to the curves recorded under brightfield illumination (Figure 3). This demonstrated the feasibility of correlated

FL-FluidFM microscopy without any disturbance of the force-curve data. Nevertheless, it has to be mentioned that the integration of the fluorescence light also involved some challenges. As previously stated, it is well known that the coincidence of cantilever and fluorescent light can cause disturbances in data acquisition, both in terms of FL and force-curve acquisition. This was also the case in the present study, which had to deal with both cantilever oscillation and cantilever luminescence using dual-excitation or blue light (475 nm) illumination. In this context, Kassies et al. (2005)[28] determined high photoluminescence for cantilevers made of silicon nitride (Si_3N_4), which is consistent with our observations regarding a wavelength of 475 nm. Here, the cantilever showed a strong autoluminescence overlapping the green paxillin signal and, therefore, hindering a removal by spectral filtering (Figure 4b,d). However, the excitation of F-actin filaments revealed no visible luminescence of the cantilever (Figure 4c) which contrasts with the study of Lulevich et al. (2005).[29] They used a commercial silicon nitride AFM cantilever as a light source by illuminating it with either 488 or 532 nm wavelength, both causing photoluminescence. They further suggested that dangling bonds or photoluminescent silicon nanocrystals within the silicon nitride could be the reason for the arising photoluminescence of Si_3N_4 cantilevers.[29] However, this is countered by the study of Kistner et al. (2011),[30] which identified the silicon nitride itself as responsible for the photoluminescence. To further investigate these effects, we additionally tested different excitation wavelengths in our setup and observed effects of cantilever luminescence in the case of ultra-violet light and none for a wavelength of 630 nm (Figure S4, Supporting Information). Summarized, this phenomenon is not yet fully understood and still needs some further research, which is beyond the scope of this publication.

Besides the effect of cantilever luminescence, we also dealt with the impact of cantilever oscillation (Figure 4f). In this context, Friedrichs et al.[13b] already claimed the simultaneous collection of force-data and fluorescence images is impossible in most cases due to fluorescence light-induced cantilever bending. Furthermore, Cazaux et al. (2015)[13a] revealed a correlation between the material cantilever composition and the wavelength and intensity of the used excitation light, resulting in an AFM/fluorescence signal coupling. They determined a stronger reaction for gold-coated than for uncoated cantilevers causing a spurious deflection for visible excitation light (470 nm), in particular, sparking a strong reaction.[13a] In relation to our study, this could be an explanation for the pronounced cantilever oscillation that occurred under dual-channel illumination (Figure 4f), where 475 and 555 nm were switched on and off alternately. This resulted in a sudden increase in force followed by a slow cantilever relaxation. However, comparing this force-curve with the ones recorded under single-channel illumination (Figure 4e: 555 nm and Figure S5, Supporting Information: 475 nm), there was not even a hint of interference, suggesting that the triggering factor is more the switching of the channels than the beams themselves. Nevertheless, to precisely determine the cause of the sinusoidal signal, a systematic investigation of experimental parameters like excitation wavelength, exposure time, or intensity are necessary which are part of our current research and beyond the scope of this publication. In the end, by focusing on the visualization of F-actin filaments, we were able to perform proof-of-principle experiments using combined FL-FluidFM for the first time and, therefore, demonstrated the correlated and simultaneous feasibility of force-curve acquisition and optical tracking of fluorescently labeled cells.

We also presented the first approach of correlated data analysis. Since the implementation of SCFS into AFM in 2008 by Helenius et al., the concept of cell adhesion and its biomechanics was described by a variety of research groups.[4b,6a,13b,24,26] Up to now, the focus was on the analysis of force-curves in particular, as these provide information about cell adhesion specific parameters, like the overall binding strength, viscous and elastic cellular deformation or the rupture of adhesion bonds.[4b,6a,13b] However, confirming these concepts in terms of real-time optical tracking of a cell was still missing. To fill this gap, our approach of data analysis highlights the matching of identified force-jumps with corresponding and visible cellular unbinding events and, therefore, provides new insights into the biomechanics of cell adhesion.

In addition to the already discussed effects of spurious cantilever bending and photoluminescence, the synchronous performance of measurements was also a challenge in establishing a reliable and correlative data analysis. This time-dependent correspondence between two separated methods can be quite complex, which might be a reason why many multifunctional devices, so far, perform their measurements in a sequential manner and superimpose their data afterward.[12a,31] While this has the advantage that a synchronized performance is not necessary, it also has the disadvantage that possible biological processes or cellular changes occurring in the meantime cannot be captured. In contrast, this study realized a real concurrent performance of two technologies by manually starting both measurements at the same time and, therefore, providing complementary information about cell adhesion forces and their biomechanics at once. To consider a possible delay between the two software, the last detachment step was determined as a reference point. This step could be clearly identified in both data sets, guaranteeing a consistent starting point for data correlation. We are aware that our presented evaluation method to correlate fluorescence imaging and mechanical detachment steps is a proof-of-principle study and has to be improved, for example, by using algorithms. Nevertheless, an unambiguous assignment between force-jumps and visible unbinding events was possible. Similar to Selhuber-Unkel et al. (2010)[26] who combined AFM with FL for investigating the intermolecular spacing of integrin during cell detachment, our study allowed the investigation of the de-adhesion process by optical tracking of the unbinding of F-actin filaments, which represent a direct link to focal contacts.[19a,32] This correlative analysis revealed a connection between characteristic force-steps and the cellular region of unbinding spreading from the inside to the outside. After starting the detachment process, the force rapidly increased until the MDF was reached within a few seconds. This could be referred to as a cellular stretching of the area around the nucleus, where the cell is immobilized and sucked onto the cantilever tip (Figure 5d and Video S1, Supporting Information). This is consistent with the study of Cohen et al. (2017),[16] which stated that the MDF

generally appears at a short separation distance between cell and substrate. Analogous to the investigation of Friedrichs et al. (2013),[13b] our results demonstrated a time-dependent shrinkage of cellular contact area until only the cell edge is in contact with the surface (Figure 5d). Moreover, the exemplary force-curve, illustrated in Figure 5a, revealed a high number of discrete force-steps. A distinction can be made between two different types of steps: a) the so-called jumps/rupture events ("j" events) and b) the tether events ("t" events). Whereas "j" events are characterized by a preceding ramp-like increase in force, force-plateaus prior to a step are visible, when pulling a tether.[2a,4b] The latter predominantly appears in the final phase of a detachment process, when membrane-nanotubes (tether) are extracted out of the cellular cortex.[4b,13b] On the other hand, "j" events mostly occur after exceeding the MDF. They represent the intracellular rupture of adhesive bonds that remain anchored to the cytoskeleton.[4b] These two concepts of cellular unbinding could also be observed in our studies, showing "j" events in the middle as well as force-plateaus at the end of a force-curve. Furthermore, this observation was also supported by an asymptotical change of slope distribution of linearly fitted detachment steps (Figure S2, Supporting Information). Regardless of the number of detachment steps within a cellular de-adhesion, the highest negative slopes were visible at the beginning of a detachment process, followed by a decline that settled around zero at the end. Besides this force-curve analysis, our studies also confirmed the linkage between the type of force-step and the region of cellular unbinding by visualizing the transition from a full-body contact zone to a contact zone where the cell membrane is connected to the surface exclusively (Figure 5d and Video S1, Supporting Information). Moreover, the specific optical-tracking of fluorescently labeled F-actin filaments enabled the correlation of a high number of discrete force-steps with the corresponding spots of cellular unbinding, for the first time.

4. Conclusion

This study aimed at the correlation of the FluidFM technology and the FL for real-time simultaneous quantification of adhesion forces and visualization of corresponding cellular detachment steps. The application of this multifunctional device was tested on single REF52 cells, fluorescently labeled for paxillin and F-actin, and well known for the formation of mature focal contacts. The adaptation of the optical detection path via PIFOC and oil immersion objective ensured high focus stability and high optical resolution throughout an entire cell detachment. Therefore, a real-time optical-tracking of a whole de-adhesion process without negatively affecting force-curve's sensitive data acquisition was feasible. Furthermore, the integration of FL allowed the visualization of cells on a sub-cellular level. Thus, we achieved the simultaneous recording of force-curves and fluorescence time-series that tracked the entire detachment process of a cell. Here, the unbinding of F-actin filaments was clearly visible, spreading from the inside to the cellular periphery and, therefore, confirming the classification of force-steps into intracellular rupture events and membrane nanotubes occurring at the final phase of a detachment process. We are convinced that the correlation of FluidFM technology and FL represents a powerful new approach, enabling the concurrent performance of force-curve quantification and detachment step visualization and, therefore, revealing new insights into the mechanobiology of cell adhesion.

5. Experimental Section

Cell Culture: For all cell detachment experiments, adherent REF52 cells stably expressing paxillin-YFP (kindly provided by the laboratory of Alexander Bershadsky at Weizmann Institute of Science, Israel) were cultivated in Dulbecco's Modified Eagle Medium (DMEM-GlutaMAX, Life Technologies, USA) supplemented with 10% fetal bovine serum (FBS, Sigma-Aldrich Inc., St. Louis, USA), 1% penicillin/streptomycin (10 000 U mL^{-1}, Life Technologies, USA), and 1% HEPES buffer (1 M, Sigma-Aldrich, Inc., St. Louis, USA). The cells were sub-cultured twice a week and stored at 37 °C with 5% CO_2 supply.

Transient Transfection: REF52-paxillin-YFP cells were additionally transiently transfected with LifeAct-mCherry (kindly provided by the laboratory of Alexander Bershadsky at Weizmann Institute of Science, Israel), a fusion protein that specifically binds to F-actin filaments. Lipofectamine2000 (Thermo Fisher Scientific Inc., Waltham, USA) was used as a transfection reagent. The preparation of the lipid-DNA-complex was performed with Opti-MEM (Thermo Fisher Scientific Inc., Waltham, USA) as reduced serum media. One day before transfection, the cells were seeded at a density of 2000 to 3000 cells cm^{-2} on 40 mm glass-bottom dishes (WillCo Wells B.V., Amsterdam, Netherlands) and mounted with 1 mL of serum-free culture media. On the day of transfection, a lipid-DNA-complex containing 1 µg DNA was added to the cells and incubated at 37 °C. After 5 to 6 h, the transfection media was replaced by the corresponding culture media and stored in the incubator at 37 °C. The next day, the transfected cells were analyzed at the FL-FluidFM system. Right before the experimental investigation, the cells were carefully rinsed two to three times with 1x Dulbecco's phosphate-buffered saline (PBS) (Sigma-Aldrich Inc., St. Louis, USA) followed by coverage with FluoroBrite solution (Thermo Fisher Scientific Inc., Waltham, USA) providing a reduction of background signal and higher signal-to-noise-ratio (SNR). Each sample was used for cellular detachment experiments for a maximum of 1.5 to 2 h.

Cantilever Preparations: FluidFM technology was performed using silicon-based microfluidic probes with a nominal spring constant of 2 N m^{-1} (FluidFM micropipette cantilever, Cytosurge AG, Glattbrugg, Switzerland). These tipless cantilevers were equipped with a microchannel and an aperture of 8 µm in diameter at the free end. On the other side, the micropipette was connected to a pressure system (Cytosurge AG, Glattbrugg, Switzerland). Before an experiment, each cantilever was prepared by calibrating the spring constant as well as the deflection sensitivity via build-in procedures of the Cytosurge and Nanosurf software. For an application in a complete liquid surrounding, the fluid reservoir of the FluidFM cantilever was loaded with HEPES-2 buffer (10 mM HEPES supplemented with 150 mM sodium chloride (NaCl) solution, pH = 7.4) and pushed into the microchannel by applying a slight over pressure. The alignment of the microfluidic probe was performed by using a near-infrared super-luminescence-diode (NIR SLD). Its low-coherence length enabled compatibility with simultaneous FL. The piezo-regulated movement of the cantilever was controlled via a closed feedback-loop within the scan head.

FL-FluidFM Data Acquisition: FL-FluidFM data acquisition was operated on separate computers for independent but simultaneous control of the correlated methods. FL was performed by using ZEN 2.6 as imaging software of ZEISS (Carl ZEISS AG, Oberkochen, Germany). The control unit of FluidFM experiments was composed of two software: the Cytosurge-ARYA for cantilever alignment and defined cell detachment workflow, and the C3000 controller unit (Nanosurf GmbH, Langen, Germany) for monitoring the cantilever deflection as well as the movement of the 100 µm Z-stage and PIFOC.

Prior to each measurement, the sample stage was set to the highest position of +50 µm, followed by a cantilever approach with 5 µm s^{-1} until a set point of 30 to 50 nN was reached. A defined working distance between cantilever and a targeted cell was achieved by subsequently retracting the Z-stage by 20 µm. With starting the FL-FluidFM measurement, the Z-stage moved upwards until cantilever and cell were in contact and a setpoint between 30 and 50 nN was reached, followed by the immobilization of the cell by applying a negative pressure of −400 to −500 mbar. A stable sealing between micropipette and cell was achieved by a pause of 2 to 3 s in which the sample stage position and force were kept constant. Afterwards, while maintaining a constant suction pressure, the 100 µm Z-stage was retracted with a speed of 2 µm s^{-1} until the lowest stage position of −50 µm was reached. During this backward movement, the detachment process of an immobilized cell was recorded with a frequency of 1024 Hz, while at the same time, the fluorescence microscope acquired a time-series of 60 to 70 s. The acquisition of all time-series was performed by using an excitation wavelength of 555 nm. Its intensity was set to 100% and the exposure time was within a range of 200 to 300 ms. The acquisition of dual-channel fluorescence images was accomplished by combining 555 nm with 475 nm excitation light. The exposure time was set to 500 ms in both cases, whereas the intensity of the blue laser was limited to 40%. After each experiment, the cantilever was cleaned by rinsing it for 1 min with sodium dodecyl sulfate (SDS) followed by several washing steps with ultrapure water. All FL-FluidFM measurements were performed at room temperature and in FluoroBrite solution as an experimental surrounding medium.

Force-Curve Processing: The recorded data of a cellular detachment was extracted in Excel. Each section of the detachment procedure, meaning approach, pause/immobilization, and retraction was given as data in the form of cantilever deflection and Z-stage position, depending on the time. For the graphical illustration of a force-time curve, the data was processed using OriginPro2020. Since the force was proportional to the deflection, Hook's Law

$$F = k_{\text{Calib}} \cdot x = k_{\text{Calib}} \cdot d \cdot \delta_{\text{Calib}} \tag{1}$$

was applied. Here, the calibrated spring constant k_{Calib} [N m^{-1}] was multiplied by the cantilever deflection x [m], which was composed of the deflection signal d [V] and the calibrated deflection sensitivity δ_{Calib} [m V^{-1}]. With this, a whole cell detachment process could be displayed as force-curve over time.

Detachment Step Analysis: Single unbinding steps of a retraction-curve were analyzed using OriginPro2020. Each force-jump that was preceded by either a ramp-like change in force or a plateau was defined as a definite detachment step and manually analyzed via a linear fit. The respective slope with standard deviation was automatically calculated by a software implemented tool. To limit the fitting area, two markers were set, one at the beginning and one at the end of the step. In this way, all slopes within a detachment process could be displayed as a slope-detachment step graph.

Correlated Analysis of FL-FluidFM Data: Force-curves were analyzed as described before. The data processing of recorded time-series was performed using ZEN 3.0 and ImageJ. After adjusting the fluorescent contrast, the relative time of a visualized detachment process was displayed, using a software-implemented tool. Unambiguous matching of identified detachment steps and spots of cellular unbinding was achieved by using the last force-step and its corresponding time as a reference and starting point for data reconciliation. A possible temporal delay between the two data sets was compensated by considering the time difference at each correlated unbinding process.

Supporting Information

Supporting Information is available from the Wiley Online Library or from the author.

Acknowledgements

This work was financially supported by the European Union (European Fund for Regional Development, EFRE-Bayern 2014–2020, Bio3D Druck project 20-3400-2-10).

Open access funding enabled and organized by Projekt DEAL.

Conflict of Interest

The authors declare no conflict of interest.

Data Availability Statement

The data that support the findings of this study are available in the supplementary material of this article.

Keywords

cell adhesion, cellular detachment, correlated microscopy, fluidic force microscopy, fluorescence microscopy

Received: February 6, 2022
Revised: April 8, 2022
Published online: June 25, 2022

[1] a) H. Sanchez, R. Kanaar, C. Wyman, *Ultramicroscopy* **2010**, *110*, 844; b) Z. Sun, H. Y. Tan, P. R. Bianco, Y. L. Lyubchenko, *Sci. Rep.* **2015**, *5*, 9625.

[2] a) P.-H. Puech, K. Poole, D. Knebel, D. J. Muller, *Ultramicroscopy* **2006**, *106*, 637; b) A. Simon, M.-C. Durrieu, *Micron* **2006**, *37*, 1; c) M. Benoit, D. Gabriel, G. Gerisch, H. E. Gaub, *Nat. Cell Biol.* **2000**, *2*, 313.

[3] a) B. M. Gumbiner, *Cell* **1996**, *84*, 345; b) M. S. Steinberg, *Science* **1963**, *141*, 401.

[4] a) P. L. Ryan, R. A. Foty, J. Kohn, M. S. Steinberg, *Proc. Natl. Acad. Sci. USA* **2001**, *98*, 4323; b) A. V. Taubenberger, D. W. Hutmacher, D. J. Muller, *Tissue Eng., Part B* **2014**, *20*, 40.

[5] a) E. Farahani, H. K. Patra, J. R. Jangamreddy, I. Rashedi, M. Kawalec, R. K. Rao Pariti, P. Batakis, E. Wiechec, *Carcinogenesis* **2014**, *35*, 747; b) S. M. Albelda, *Lab Invest.* **1993**, *68*, 4; c) A. Sancho, I. Vandersmissen, S. Craps, A. Luttun, J. Groll, *Sci. Rep.* **2017**, *7*, 46152.

[6] a) J. Helenius, C.-P. Heisenberg, H. E. Gaub, D. J. Muller, *J. Cell Sci.* **2008**, *121*, 1785; b) O. Guillaume-Gentil, E. Potthoff, D. Ossola, C. M. Franz, T. Zambelli, J. A. Vorholt, *Trends Biotechnol.* **2014**, *32*, 381.

[7] R. Schubert, N. Strohmeyer, M. Bharadwaj, S. P. Ramanathan, M. Krieg, J. Friedrichs, C. M. Franz, D. J. Muller, *FEBS Lett.* **2014**, *588*, 3639.

[8] T. F. D. Fernandes, O. Saavedra-Villanueva, E. Margeat, P.-E. Milhiet, L. Costa, *Sci. Rep.* **2020**, *10*, 18385.

[9] C. G. Galbraith, J. A. Galbraith, *J. Cell Sci.* **2011**, *124*, 1607.

[10] a) J. E. Shaw, J. Oreopoulos, D. Wong, J. C. Y. Hsu, C. M. Yip, *Surf. Interface Anal.* **2006**, *38*, 1459; b) W. Christenson, I. Yermolenko, B. Plochberger, F. Camacho-Alanis, A. Ros, T. P. Ugarova, R. Ros, *Ultramicroscopy* **2014**, *136*, 211.

[11] A. I. Gómez-Varela, D. R. Stamov, A. Miranda, R. Alves, C. Barata-Antunes, D. Dambournet, D. G. Drubin, S. Paiva, P. A. A. De Beule, *Sci. Rep.* **2020**, *10*, 1122.

[12] a) P. D. Odermatt, A. Shivanandan, H. Deschout, R. Jankele, A. P. Nievergelt, L. Feletti, M. W. Davidson, A. Radenovic, G. E. Fantner, *Nano Lett.* **2015**, *15*, 4896; b) J. V. Chacko, F. C. Zanacchi, A. Diaspro, *Cytoskeleton* **2013**, *70*, 729.
[13] a) S. Cazaux, A. Sadoun, M. Biarnes-Pelicot, M. Martinez, S. Obeid, P. Bongrand, L. Limozin, P.-H. Puech, *Ultramicroscopy* **2016**, *160*, 168; b) J. Friedrichs, K. R. Legate, R. Schubert, M. Bharadwaj, C. Werner, D. J. Müller, M. Benoit, *Methods* **2013**, *60*, 169.
[14] E. Potthoff, O. Guillaume-Gentil, D. Ossola, J. Polesel-Maris, S. LeibundGut-Landmann, T. Zambelli, J. A. Vorholt, *PLoS One* **2012**, *7*, e52712.
[15] A. Meister, M. Gabi, P. Behr, P. Studer, J. Voros, P. Niedermann, J. Bitterli, J. Polesel-Maris, M. Liley, H. Heinzelmann, T. Zambelli, *Nano Lett.* **2009**, *9*, 2501.
[16] N. Cohen, S. Sarkar, E. Hondroulis, P. Sabhachandani, T. Konry, *Talanta* **2017**, *174*, 409.
[17] P. Saha, T. Duanis-Assaf, M. Reches, *Adv. Mater. Interfaces* **2020**, *7*, 2001115.
[18] a) P. Dörig, P. Stiefel, P. Behr, E. Sarajlic, D. Bijl, M. Gabi, J. Vörös, J. A. Vorholt, T. Zambelli, *Appl. Phys. Lett.* **2010**, *97*, 023701; b) G. Charras, A. S. Yap, *Curr. Biol.* **2018**, *28*, R445.
[19] a) P. Kanchanawong, G. Shtengel, A. M. Pasapera, E. B. Ramko, M. W. Davidson, H. F. Hess, C. M. Waterman, *Nature* **2010**, *468*, 580; b) H. Deschout, I. Platzman, D. Sage, L. Feletti, J. P. Spatz, A. Radenovic, *Biophys. J.* **2017**, *113*, 2508.
[20] C. Smith, *Nature* **2012**, *492*, 293.
[21] a) A. B. Mathur, G. A. Truskey, W. M. Reichert, *Biophys. J.* **2000**, *78*, 1725; b) J. E. Shaw, R. F. Epand, R. M. Epand, Z. Li, R. Bittman, C. M. Yip, *Biophys. J.* **2006**, *90*, 2170.
[22] a) O. Guillaume-Gentil, E. Potthoff, D. Ossola, P. Dorig, T. Zambelli, J. A. Vorholt, *Small* **2013**, *9*, 1904; b) O. Guillaume-Gentil, R. V. Grindberg, R. Kooger, L. Dorwling-Carter, V. Martinez, D. Ossola, M. Pilhofer, T. Zambelli, J. A. Vorholt, *Cell* **2016**, *166*, 506.
[23] O. Guillaume-Gentil, T. Zambelli, J. A. Vorholt, *Lab Chip* **2014**, *14*, 402.
[24] P. Wysotzki, A. Sancho, J. Gimsa, J. Groll, *Colloids Surf.* **2020**, *190*, 110894.
[25] a) K. Beicker, E. T. O'Brien, M. R. Falvo, R. Superfine, *Sci. Rep.* **2018**, *8*, 1504; b) P. Bondia, S. Casado, C. Flors, *Methods Mol. Biol.* **2017**, *1663*, 105.
[26] C. Selhuber-Unkel, T. Erdmann, M. Lopez-Garcia, H. Kessler, U. S. Schwarz, J. P. Spatz, *Biophys. J.* **2010**, *98*, 543.
[27] A. G. Nagy, J. Kaman, R. Horvath, A. Bonyar, *Sci. Rep.* **2019**, *9*, 10287.
[28] R. Kassies, K. O. van der Werf, A. Lenferink, C. N. Hunter, J. D. Olsen, V. Subramaniam, C. Otto, *J. Microsc.* **2005**, *217*, 109.
[29] V. Lulevich, C. Honig, W. A. Ducker, *Rev. Sci. Instrum.* **2005**, *76*, 123704.
[30] J. Kistner, X. Chen, Y. Weng, H. P. Strunk, M. B. Schubert, J. H. Werner, *J. Appl. Phys.* **2011**, *110*, 023520.
[31] P. R. Laskowski, M. Pfreundschuh, M. Stauffer, Z. Ucurum, D. Fotiadis, D. J. Muller, *ACS Nano* **2017**, *11*, 8292.
[32] C. M. Franz, D. J. Muller, *J. Cell Sci.* **2005**, *118*, 5315.